

Received December 7, 2020, accepted December 16, 2020, date of publication December 21, 2020,  
date of current version December 31, 2020.

Digital Object Identifier 10.1109/ACCESS.2020.3045934

# Mission-Oriented 3D Path Planning for High-Altitude Long-Endurance Solar-Powered UAVs With Optimal Energy Management

XIANGYU WANG<sup>1,2</sup>, YANPING YANG<sup>1</sup>, (Member, IEEE), DI WU<sup>1</sup>, ZIJIAN ZHANG<sup>1</sup>,  
AND XIAOPING MA<sup>1</sup>

<sup>1</sup>Institute of Engineering Thermophysics, Chinese Academy of Science, Beijing 100190, China

<sup>2</sup>University of Chinese Academy of Science, Beijing 100190, China

Corresponding author: Zijian Zhang (zhangzijian@iet.cn)

This work was supported in part by the National Natural Science Foundation of China under Grant 61901448, Grant 61871401, and Grant 12002340; and in part by the China Postdoctoral Science Foundation under Grant 2019TQ0321.


**ABSTRACT** The conversion efficiency of solar energy and the capacity of energy storage batteries are the key technologies limiting the development of solar-powered aircraft. In this paper, a mission-oriented design for the 3-dimensional (3D) path planning of solar-powered unmanned aerial vehicles (SP-UAVs) using limited solar energy to maximize the mission effectiveness is presented. Based on the solar radiation received model, the energy model, and the kinetic and kinematic model of the SP-UAV, a task planning problem oriented to multiobjective optimization is proposed. Both the pseudospectral and colony algorithms are proposed to search for the optimal mission path, and their joint optimization is employed to realize continuous flight and improve the flight mission capabilities. Explicitly, a multiobjective joint strategy is developed, including maximum power ascending, maximum range flight, maximum glide endurance, and minimum power level flight at night. Numerical and simulation results indicate that our proposed design outperforms the existing approaches not only in solar energy utilization but also in universality.

**INDEX TERMS** High-altitude long-endurance aircraft, solar-powered UAV, energy management strategy, multidisciplinary optimization, path planning.

## I. INTRODUCTION

Recently, high-altitude long endurance (HALE) solar-powered unmanned aerial vehicles (SP-UAVs) have received extensive attention in the aerospace community due to their wide applications in civilian and military fields [1]–[6]. However, weak energy systems, such as the low efficiencies of photovoltaic cells and insufficient battery capacities, strongly limit the endurance of HALE SP-UAVs as well as the power of mission loadings, which limits the prospects of HALE SP-UAVs [2]–[5]. Due to these undesirable energy systems, a number of researchers have turned to alternative methods to improve HALE SP-UAV capabilities.

Klesh *et al.* first propose time-based flight attitude control to maximize solar energy collection since the absorptivity of solar cells changes with the sunlight incident angle. An analytical solution of the optimal flight path is presented by

The associate editor coordinating the review of this manuscript and approving it for publication was Haibin Sun .

Klesh *et al.*, and the results show that an SP-UAV's capabilities can be improved if the solar energy collection model is coupled considering the aircraft kinematics model. A nondimensional parameter, the power ratio, is also proposed to predict the optimal aircraft state. However, Klesh *et al.*'s work is based on the assumption that the aircraft is in a quasi-static equilibrium state at a constant altitude, which cannot completely exploit the benefits of both the sunlight incident angle and SP-UAV attitude angle. Optimal path planning at a constant height is studied by Huang *et al.* [10] for the scenario of tracking a moving ground target. A coupled method including particle swarm optimization (PSO) and receding horizon control (RHC) is applied. Extensive results are presented that show that solar aircraft can successfully follow a ground target moving in the wide speed range of 7 to 30 m/s. However, similar to Klesh *et al.*'s work, Huang *et al.* only consider an invariable height flight, which distorts the 3D aircraft motion into a two-dimensional case. Spangelo *et al.* [9] further extend Klesh *et al.*'s idea and

introduce aircraft altitude variations into the optimization of flight path planning. They point out that the optimal average power for dynamic flight paths exceeds the optimal average power for flight paths that have constant speed and constant altitude by as much as 30%, which brings the HALE SP-UAV energy collection optimization into a 3D region.

In addition to improving solar energy collection by controlling flight attitude, Gao *et al.* [13] argue that a reasonable utilization of gravitational potential energy might enhance the capabilities of HALE SP-UAVs. They further analyzed the equivalence of gravitational potential energy and rechargeable battery weight [14] and proposed an energy management strategy during a one-day-night cycle [15], [16]. Lee *et al.* [19] proved that using gravitational potential energy storage for path planning can realize 48-hour nonstop flight of a low-altitude SP-UAV. Sun *et al.* [20] further extend Gao *et al.*'s opinion and discuss the usage of gravitational potential energy storage to reduce the aircraft's night cruising time while decreasing the weight of the energy storage battery. Wang *et al.* [18] integrated two methods of flight attitude control and gravitational potential energy storage. Compared with the current constant-altitude constant-velocity flight strategy, the optimized flight strategy can reduce the energy consumption of SP-UAVs but lacks practical application scenarios. Specifically, Huang *et al.* [17] study the path planning of an SP-UAV in 3D space and combine the application scene with fixed targets but fix the flight path on the surface of a cylinder, which actually distorts the 3D model into a two-dimensional case. To the best of our knowledge, apart from the work outlined in [17], the combination and application of the two strategies, especially in 3D flight path planning combined with application scenarios, has been largely underexplored.

3D path planning combined with the application scene has the difficulties associated with being multiobjective, multiconstraint, and multicoupled. To overcome the aforementioned difficulties, we propose an integrated optimization model to investigate the problem of 3D path planning optimization based on the HALE SP-UAV application scenario. First, for the nonlinear optimal control problem with process constraints and terminal constraints in complex task scenarios, the Gauss pseudospectral method (GPM) is introduced to discretize the state equations and constraint equations, which has been thoroughly examined and proven to have certain advantages in terms of computing efficiency and approximation accuracy [9], [15], [18]. Therefore, the GPM is applied in the optimal path planning problem of SP-UAVs [15], [18], [20]. However, the path planning of SP-UAVs is highly related to the flight environment, and it is difficult for the GPM to be coupled with the constraints of complex external scenes. Then, the ant colony algorithm is innovatively introduced to execute path planning in application scenarios. Ant colony optimization (ACO) is a population-based approach that has been successfully applied to several NP-hard combinatorial optimization problems [30], [31]. Through path optimization, an optimal 3D flight path of a near-space SP-UAV

that meets the energy requirements of the cruise state and mission state can be found. Additionally, multiconstraint, multiobjective, point-to-point path planning optimization is achieved by analyzing the feasible range of continuous flight at different latitudes and seasons.

Against the above rationale and the inspirational contributions of [17], the contributions of this paper can be summarized as follows:

- 1) We propose a path planning algorithm suitable for SP-UAV application scenes with higher degrees of freedom. Oriented by the task application, we solve the problem of the optimal path for complex tasks with finite energy. To find the optimal path planning for different tasks, the point-to-point method is used to discretize the task path, and the maximum solar radiation path is obtained by using this method.
- 2) The flight path problem is optimized in 3D space. Increases in the dimensions and the constraints of the task result in a significant increase in the complexity. The energy requirements in the cruise state and mission state are studied, and the optimal 3D flight path of an SP-UAV in near space is obtained through the proposed joint path optimization algorithm.
- 3) The GPM algorithm is innovatively combined with a heuristic algorithm. For the nonlinear optimal control problem with process constraints and terminal constraints, the GPM is employed to discretize the state equations and constraint equations, and the ant colony algorithm is used to solve the problem of path planning in application scenarios.

The remaining part of the paper proceeds as follows. Section II begins by laying out the solar radiation received model and formulating our optimization problem. Section III is concerned with the heuristic algorithm for multi-/single-objective path optimization, followed by validation of the methodology used for this study compared with the existing method. Section IV presents the numerical results and performance analysis. Section V provides our concluding remarks.

## II. SYSTEM MODEL AND PROBLEM FORMULATION

Communication relay and information acquisition are an important part of HALE SP-UAV mission scenarios. Based on the characteristics of the platform in near space, the system modeling of the mission process mainly consists of four parts: the solar radiation received model, the energy model, the dynamics and aerodynamic model, and the application scenarios model. The symbols used in this paper are listed in Table 1.

### A. SOLAR RADIATION RECEIVED MODEL

In this section, a solar radiation received model that combines an SP-UAV dynamics model with a solar irradiance model is introduced. Based on the solar radiation model that evolved from [21]–[27], the solar energy obtained by the solar-powered aircraft at any time, any place, and any flying attitude can be estimated.

TABLE 1. Symbols and abbreviations.

Parameter	Definition	Parameter	Definition
$m$	mass	$GS$	ground coordinate system
$n_s$	unit vector on the line between the sun and the earth	$I_{tot}$	total irradiance
$\gamma_s$	sun's azimuthal angle	$I_{dif}$	scattered irradiance
$\alpha_s$	angle of the sun's altitude from the center of the earth to the center of the sun	$I_{beam}$	direct irradiance
$n_{pm}$	external normal unit vector of the photovoltaic module plane	$I_{on}$	solar irradiance outside the atmosphere on the day of the year
$v$	air speed	$S_{pm}$	plane area of each photovoltaic module
$\eta_{pm}$	efficiency of the photovoltaic modules	$N_{pm}$	total number of photovoltaic modules
$\eta_{mot}$	motor efficiency	$P_{pld}$	load power
$\eta_c$	battery efficiency	$R_E$	radius of the earth
$\eta_{prop}$	propeller efficiency	$P_{av}$	avionics power
$\gamma$	flight path angle	$T$	thrust
$\varphi$	bank angle	$E_{bat}$	total battery energy
$\psi$	heading angle	$SoC$	state of charge
$\alpha$	attack angle	$L$	aerodynamic lift
$\rho$	air density	$D$	aerodynamic drag
$S$	wing area	$C_L$	lift coefficient
$C_D$	drag coefficient	$C_{D0}$	zero-lift drag coefficient
$K$	aerodynamic coefficient	$R_a$	aspect ratio
$\varepsilon$	Oswald efficiency factor		

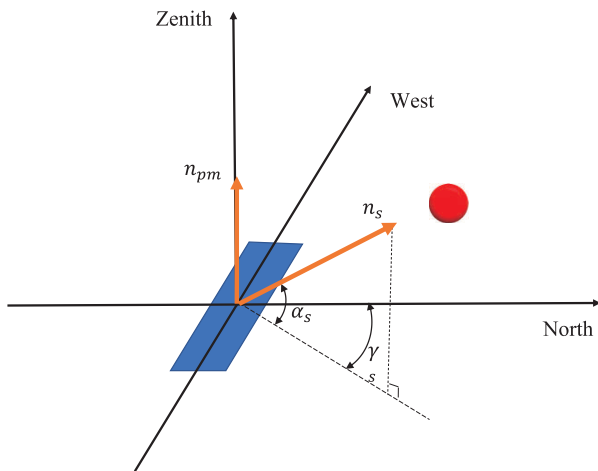


FIGURE 1. Angle between the photovoltaic module and the sun.

In Fig. 1,  $GS$  is the northeast down, which is the inertial coordinate system fixed on the earth,  $n_s$  is the unit vector pointing from the photovoltaic module to the sun, and  $\alpha_s$  is the angle between  $n_s$  and the earth plane.  $\gamma_s$  is the azimuthal angle of the sun, which refers to the angle between the projection of  $n_s$  in the ground plane and the south. In the surface coordinate system,  $n_s$  can be expressed by  $\alpha_s$  and  $\gamma_s$ :

$$n_s = (\cos \alpha_s \cos \gamma_s, \cos \alpha_s \sin \gamma_s, -\sin \alpha_s)^T, \quad (1)$$

in which  $\alpha_s$  and  $\gamma_s$  can be determined by the local latitude  $\varphi_{lat}$ , the solar declination  $\delta_s$  and the solar time  $\theta_h$ :

$$\sin \alpha_s = \sin \varphi_{lat} \sin \delta_s + \cos \varphi_{lat} \cos \delta_s \cos \theta_h. \quad (2)$$

For solar photovoltaic modules, the solar radiation energy perpendicular to the photovoltaic module can be most effectively absorbed. In Fig. 1,  $n_{pm}$  is the external normal unit vector of the photovoltaic module plane; thus, the cosine value of the incident angle of solar rays in the photovoltaic module can be expressed as  $\cos \langle n_s, n_{pm} \rangle$ . In the ground coordinate

system,  $n_{pm}$  can be determined by the attitude angle and the photovoltaic module laying angle, which can be expressed as:

$$n_{pm} = - \begin{pmatrix} \cos \psi_b \sin \theta_{pm} \cos \varphi_{pm} + \sin \psi_b \sin \varphi_{pm} \\ \sin \psi_b \sin \theta_{pm} \cos \varphi_{pm} - \cos \psi_b \sin \varphi_{pm} \\ \cos \theta_{pm} \cos \varphi_{pm} \end{pmatrix} \quad (3)$$

where  $\psi_b$  represents the yaw angle between the body coordinate axis and the  $GS$  coordinate axis and  $\theta_{pm}$  and  $\varphi_{pm}$  represent the elevation angle and roll deflection angle between the coordinate system fixed on each photovoltaic module and the body coordinate axis, respectively.

Due to the thin clouds and reduction in impurity particles in the upper atmosphere, the calculation of the solar radiation can ignore the contribution of the solar reflection irradiance. The total irradiance  $I_{tot}$  is the sum of the direct irradiance  $I_{beam}$  and the scattered irradiance  $I_{dif}$  [26]:

$$I_{tot} = I_{beam} + I_{dif}, \quad (4)$$

where the direct irradiance and the scattered irradiance can be expressed as:

$$I_{beam} = I_{on} \exp \left( - \frac{c_s \exp(-\frac{h}{h_s})}{\left[ \sin(\frac{\alpha_s + \alpha_{dep}}{1 + \alpha_{dep}/90}) \right]^{S_s + \frac{h}{h_b}}} \right), \quad (5)$$

and

$$I_{dif} = 0.8 I_{beam} \exp \left( - \frac{h}{h_s} \right), \quad (6)$$

in which  $I_{on}$  and  $\alpha_{dep}$  are given by:

$$I_{on} = G_{sc} [1 + 0.033 \cos(360n_d/365)], \quad (7)$$

and

$$\alpha_{dep} = 0.57 + \arccos [R_E / (R_E + h)], \quad (8)$$

where  $G_{sc}$  is the standard solar radiation constant,  $I_{on}$  is the solar irradiance outside the atmosphere on the day of the year,  $h$  is the flight altitude of the solar-powered aircraft, and  $R_E$  is the radius of the earth. The values of the parameters are shown in Tab. 2.

TABLE 2. Parameters of the solar radiation received model.

Parameter	Value	Definition
$G_{sc}$	1367 W/m <sup>2</sup>	Standard solar radiation constant
$c_s$	0.357	
$S_s$	0.678	Earth radius
$h_b$	40 km	
$h_s$	7 km	
$R_E$	6356.8 km	

**B. ENERGY MODEL**

Based on Eqs. (1)-(8), it can be derived that at any time, the total power  $P_{pm}$  converted by the photovoltaic modules on an SP-UAV can be expressed as:

$$P_{pm} = \sum_i^{N_{pm}} (\eta_{pm} I_{tot} \cos \langle n_s, n_{pm} \rangle S_{pm})_i, \tag{9}$$

where  $S_{pm}$  is the plane area of each photovoltaic module,  $N_{pm}$  is the total number of photovoltaic modules,  $i$  is the serial number of photovoltaic modules, and  $\eta_{pm}$  is the efficiency of the photovoltaic modules.

Therefore, the total energy input from  $t_0$  to  $t_f$  is:

$$E_{in} = \int_{t_0}^{t_f} P_{pm} dt. \tag{10}$$

The energy consumed by the SP-UAV includes the power consumption of airborne equipment, the load power consumption and the power consumption of the propulsion system, which can be expressed as:

$$P_{out} = P_{av} + P_{pld} + \frac{Tv}{\eta_{prop}\eta_{mot}}, \tag{11}$$

where  $P_{av}$  denotes the avionics power,  $P_{pld}$  is the load power,  $T$  is the thrust,  $v$  is the air speed,  $\eta_{prop}$  is the propeller efficiency, and  $\eta_{mot}$  is the motor efficiency.

Through the definition of the total battery energy  $E_{bat}$  and the battery efficiency  $\eta_c$ , the state of charge (SoC) is then updated by:

$$\frac{dSoC}{dt} = \eta_c \frac{P_{pm} - P_{out}}{E_{bat}}, \tag{12}$$

where  $0 < SoC < 1$ .

**C. DYNAMICS MODEL**

For the research of path planning, the focus is on the aircraft’s macroscopic characteristics during the flight. Therefore, a simplified mass point model can be used for research. Assuming that the aircraft flies without side slip, the dynamics equations and kinematic equations of the

SP-UAV can be expressed as follows:

$$\begin{cases} T \cos \alpha - D - mg \sin \gamma = m \frac{dv}{dt} \\ (T \sin \alpha + L) \cos \varphi - mg \cos \gamma = mv \frac{d\gamma}{dt} \\ (T \sin \alpha + L) \sin \varphi = mv \cos \gamma \frac{d\psi}{dt} \\ \frac{dx}{dt} = v \cos \gamma \cos \psi \\ \frac{dy}{dt} = v \cos \gamma \sin \psi \\ \frac{dh}{dt} = v \sin \gamma, \end{cases} \tag{13}$$

where  $m$  is the aircraft mass,  $v$  is the aircraft velocity,  $\gamma$  is the flight path angle,  $\psi$  is the heading angle,  $\varphi$  is the bank angle,  $\alpha$  is the attack angle, and  $x$ ,  $y$  and  $h$  are the aircraft position coordinates in the flat earth-fixed frame.

Parameters  $L$ ,  $D$ , and  $T$  represent the aerodynamic lift, drag and thrust, respectively:

$$\begin{cases} T = (P_{pm} - P_{av} - P_{pld})\eta_{prop}\eta_{mot}/v \\ L = \frac{1}{2}\rho S C_L v^2 \\ C_L = C_{L_0} + C_{L_\alpha} \alpha \\ D = \frac{1}{2}\rho S C_D v^2 \\ C_D = C_{D_0} + K C_L^2 \\ K = \frac{1}{\varepsilon \pi R_a}, \end{cases} \tag{14}$$

where  $\rho$  is the air density,  $S$  is the wing area,  $C_L$  is the lift coefficient,  $C_D$  is the drag coefficient,  $C_{D_0}$  is the zero lift drag coefficient,  $K$  is the induced drag factor,  $R_a$  is the aspect ratio, and  $\varepsilon$  is the Oswald efficiency factor. The lift coefficient is related to the angle of attack. In this study,  $\alpha$ ,  $\varphi$ , and  $T$  are chosen as the three control variables for changing the aircraft attitude and flight altitude.

**D. HIGH ALTITUDE LONG-TIME FLIGHT ENVIRONMENT MODEL**

Based on the application scenarios of high-altitude long-term flight, in the scenario simulated in this paper, the aircraft cruises through major cities to complete information acquisition. Nineteen major cities are selected as candidate cities for mission planning, as shown in Fig. 2.

In this scenario, each city is considered to be a single mass point. The latitude and longitude of the city determine the intensity of the illumination at that moment, and the distance between the cities needs to be used to calculate the direction and distance of the flight. Therefore, the distance and direction between cities should be converted to latitude and longitude, as generated by Eq. (15), as shown at the bottom of the next page,  $\rho_{in}$  which  $d$  and  $\zeta$  are the distance and the direction angle between city A and city B, respectively, and  $la_1$  and  $la_2$  are the latitudes of A and B, respectively; similarly,  $lon_1$  and  $lon_2$  are the longitudes of A and B, respectively.

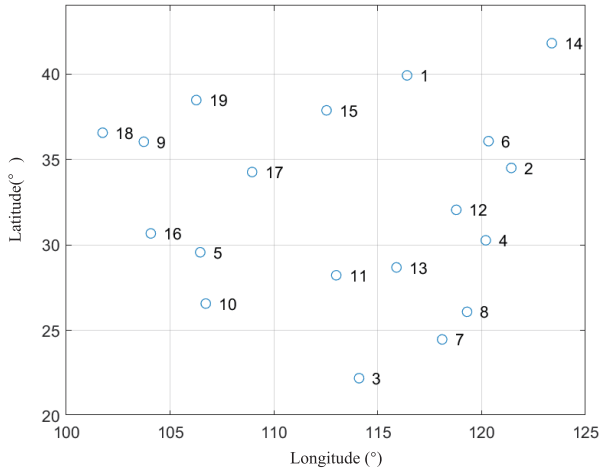


FIGURE 2. Application scenario (19 cities).

### III. HEURISTIC ALGORITHM OF MULTI-/Single-OBJECTIVE PATH OPTIMIZATION

#### A. MULTIGOAL PATH OPTIMIZATION BY THE PSEUDOSPECTRAL METHOD

Optimization problems with flight dynamics equation constraints are usually nonlinear problems of a higher order. The Gauss pseudospectral method (GPM) is applicable for solving path planning problems and has also been thoroughly examined and proven to have certain advantages in terms of computing efficiency and approximation accuracy [9], [15], [18]. The GPM uses the finite basis of a global interpolation polynomial to approximate the state and control variables at a series of discrete points [28], [29]. It uses polynomial derivation to approximate the derivatives of the state variables in dynamic equations and satisfies the dynamic equations in a series of matching points, thereby transforming differential equations into algebraic constraints. The multistage optimization problem can be solved effectively by transforming the optimal control problem into a nonlinear programming problem. Therefore, in this paper, the GPM is used to solve the flight path parameter optimization problem of the SP-UAV.

The flight strategy of the aircraft is divided into four parts based on the flight strategy using gravity potential energy storage in Fig. 3, and the energy allocation at each stage is presented in Fig. 4.

Here, the GPM is employed. Given a set of  $N = 4$  stages, the objective function of the whole stage can be summarized as:

$$\max f = t_0 - t_1 + \frac{\int_{t_1}^{t_2} v dt}{t_2 - t_1} + t_3 - t_2 + \int_{t_3}^{t_4} P_{level} dt. \quad (16)$$

As the periodic trajectory is planned to circulate day and night, the flight states in the final state of the fourth stage are set to be the beginning of the cycle; that is,  $t_4 = t_0$ .

Finally, the GPM can be used to transform the original continuous optimization problem into a defined nonlinear problem.

#### B. POINT-TO-POINT MAXIMUM SOLAR RADIATION PATH OPTIMIZATION BY THE COLONY ALGORITHM

The colony algorithm simulates the foraging behavior of ants and has been successfully applied to several NP-hard combinatorial optimization problems [30], [31]. The ant colony algorithm adopts a positive feedback mechanism, which allows the search process to quickly approximate the optimal solution.

Given a set of city areas of interest and goal coordinates, path optimization finds the optimal city node order. To minimize the distance between cities, the circular path method is a good solution to the well-known traveling salesman problem (TSP) [32], [33]; furthermore, the ant colony algorithm has great advantages in solving the TSP [34]–[36]. Therefore, based on our optimization goal of the maximum solar radiation and because solar radiation is related to time, we make improvements on the basis of the ant colony algorithm, using this improved method to solve an optimal node ordering problem that depends on task constraints to obtain the maximum global maximum solar radiation path.

Suppose the number of ants is  $m$ , the number of city nodes is  $n$ , and ant  $k$  ( $k=1, 2, \dots, m$ ) determines the next visited node according to the pheromone concentration on the connection path between cities. Let  $P_{ij}^k$  be the probability that ant  $k$  moves from node  $i$  to node  $j$  at time  $t$ . The calculation formula is:

$$P_{ij}^k = \begin{cases} 0, & s \notin allow_k \\ \frac{(\tau_{ij}(t))^\alpha (\eta_{ij}(t))^\beta}{\sum_{s \in allow_k} (\tau_{ij}(t))^\alpha (\eta_{ij}(t))^\beta}, & s \in allow_k \end{cases} \quad (17)$$

and

$$\eta_{ij}(t) = 1/d_{ij} \quad (18)$$

where  $\eta_{ij}(t)$  is the heuristic function and  $d_{ij}$  is the distance between node  $i$  and node  $j$ .  $\tau_{ij}(t)$  is the pheromone concentration and can be expressed as:

$$\begin{cases} \tau_{ij}(t+1) = (1-\rho)\tau_{ij}(t) + \Delta\tau_{ij}, & 0 < \rho < 1 \\ \Delta\tau_{ij} = \sum_{k=1}^n \Delta\tau_{ij}^k \\ \Delta\tau_{ij}^k = \begin{cases} P_{total}/Q, & \text{ant } k \text{ from node } i \text{ to node } j \\ 0, & \text{other,} \end{cases} \end{cases} \quad (19)$$

$$\begin{cases} d = 2 * R * \arcsin(\sqrt{HaverSin(|la1 - la2| + \cos(la1) * \cos(la2) * HaverSin(|lon1 - lon2|))}) \\ \zeta = \arctan \{((lon2 - lon1) * \cos(la2)) / (la2 - la1)\} \\ HaverSin(\theta) = \sin^2(\theta/2), \end{cases} \quad (15)$$

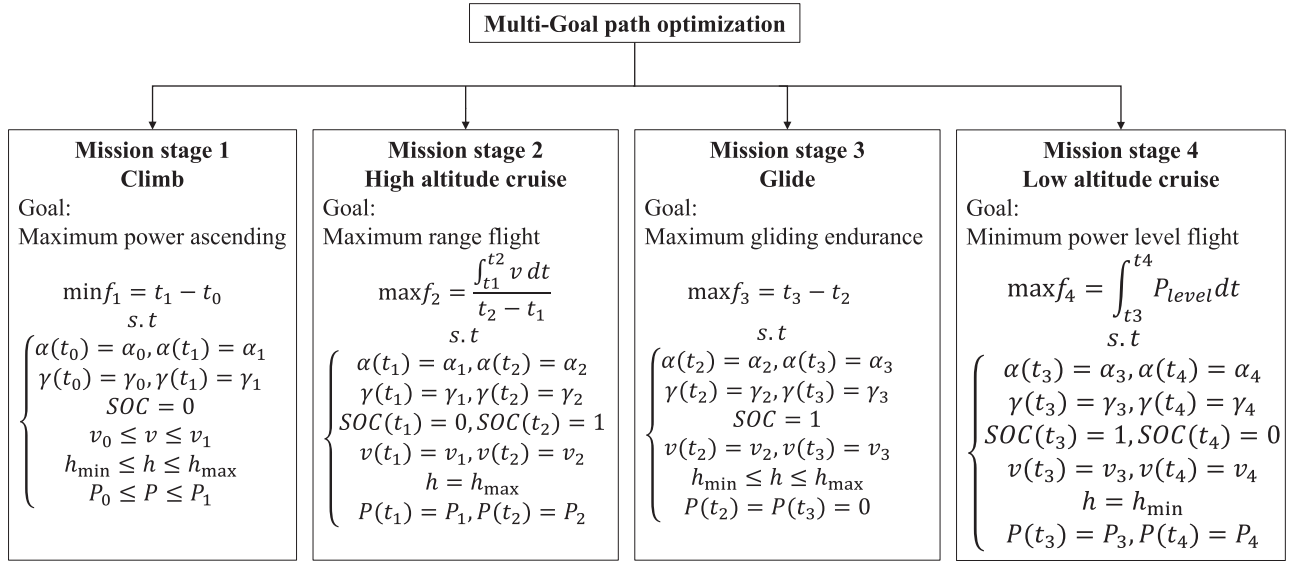


FIGURE 3. Multigoal path optimization framework.

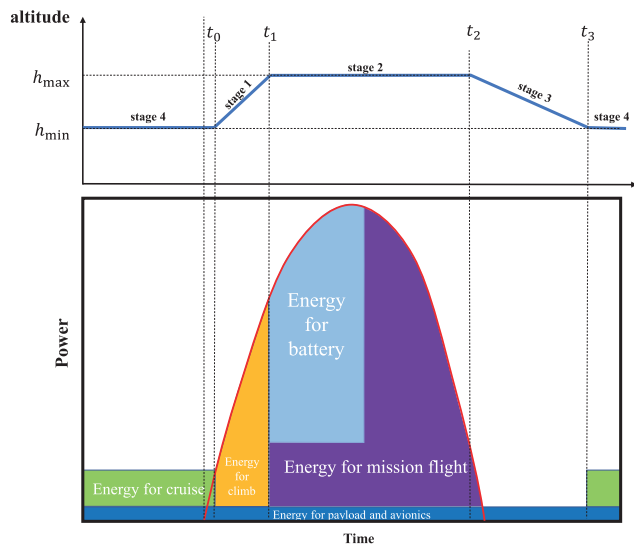


FIGURE 4. Energy distribution.

in which  $P_{total}$  is the solar radiation obtained by the ants in the path; when all ants complete a cycle, the pheromone concentration is updated.

Therefore, the problem can be mathematically stated as:

$$\begin{aligned} \max : f_p &= P_{total} \\ \text{s. t} : \sum_{i=0}^4 t_i &= 24. \end{aligned} \quad (20)$$

The parameters of the ant colony algorithm used are shown in Tab. 3.

### C. JOINT ACO AND GPM OPTIMIZATION

To address the difficulty of jointly optimizing the aircraft's multigoal path and the point-to-point maximum solar

TABLE 3. Parameters of the colony algorithm.

Parameter	Value
Maximum number of iterations	200
Number of ants	50
Number of cities	19
Pheromone importance factor	1
Heuristic function importance factor	5
Pheromone volatility factor	0.1

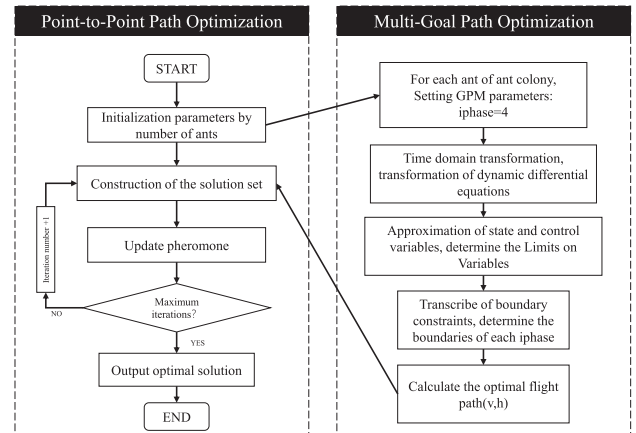


FIGURE 5. Joint optimization framework.

irradiation path, we propose a combination of the GPM and ant colony (ACO) algorithms. Through the above decomposition, the coupling problem of the SP-UAV path optimization is decomposed into a two-level optimization problem. The method of implementing ACO and the GPM for joint optimization is shown in Fig. 5. In the ACO algorithm, the optimization variable is the total solar irradiation energy. In the GPM algorithm, the optimization variables are the state variables of the flight path and the flight time of each segment.

TABLE 4. Parameters of the aircraft.

Parameter (Units)	Value
Wing area (m <sup>2</sup> )	0.776
Mass (kg)	2.6
Wing span (m)	3.2
Aspect ratio	12.9
Oswald factor	0.9
Zero-lift drag coefficient	0.006
Zero-lift coefficient	0.15
Lift coefficient (per degree)	0.1441
Propeller efficiency	0.85
Efficiency of solar battery	0.169
Electrical load power (W)	2
Mission load power (W)	1
Variator efficiency	0.95
Controller efficiency	0.95
Motor efficiency	0.85
Maximum angle of attack (°)	11

TABLE 5. Parameters of the simulation experiment.

Place: Beijing Date: Feb.1	Starting time: 9:00 am
Parameter name	Value
Flight motion height	50 m
Radius of virtual cylinder	300 m
Minimum flight height	300 m
Maximum tension	30 N

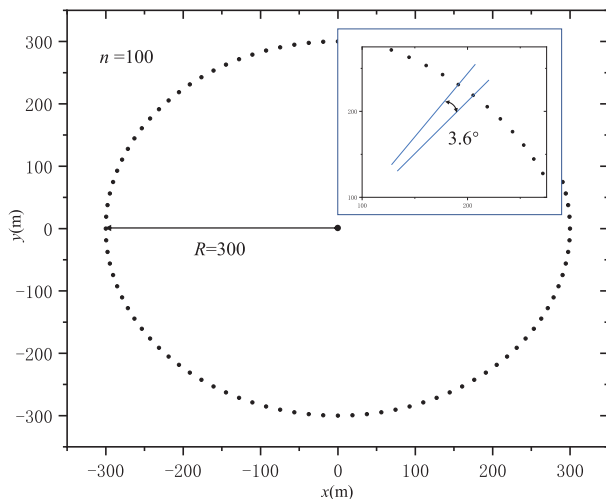


FIGURE 6. Set points.

TABLE 6. Net energy relative error.

Results of Huang[15]	Validation case	Relative error
-1388 J	-1445 J	4.1% (75 s)
1102 J	1156 J	4.9% (200 s)
1719 J	1804 J	5.0% (250 s)

IV. NUMERICAL RESULTS AND PERFORMANCE ANALYSIS

In this section, a range of representative numerical results are presented to validate our theoretical analysis. Our emphasis is on proving the reliability of the results of the joint ACO and

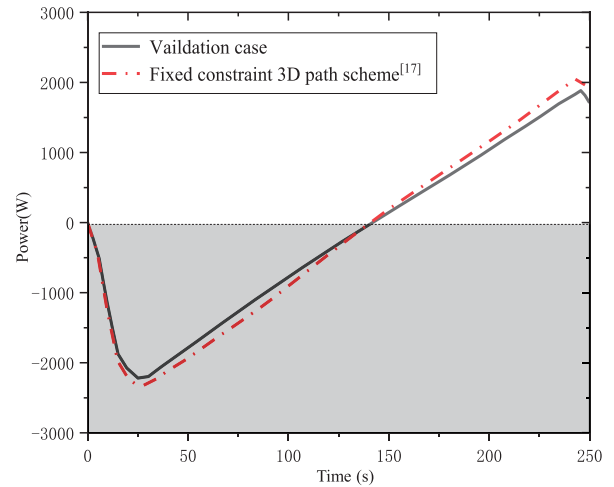


FIGURE 7. Net energy.

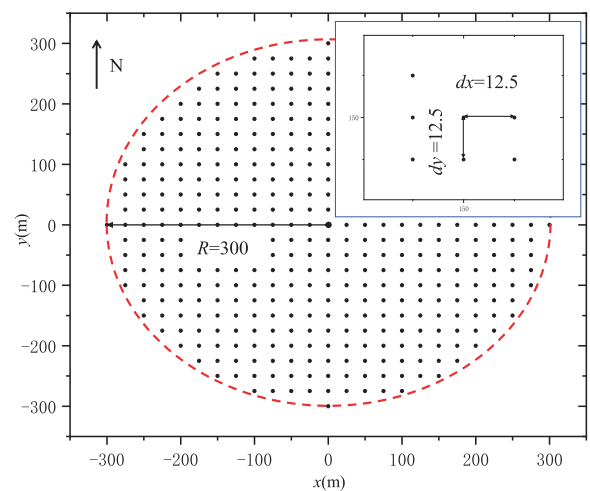


FIGURE 8. Set points.

TABLE 7. Parameters of the aircraft.

Parameter	Symbol	Value
Wing area (m <sup>2</sup> )	S	28
Mass (kg)	m	142
Total area of the photovoltaic module	S <sub>pm</sub>	20.48
Aspect ratio	R <sub>a</sub>	12.6
Oswald factor	ε	0.9
Zero-lift drag coefficient	C <sub>D0</sub>	0.02
Zero-lift coefficient	C <sub>L0</sub>	0.42
Lift coefficient (per degree)	C <sub>Lα</sub>	0.086
Photovoltaic cell efficiency	η <sub>pm</sub>	0.25
Electrical load power (W)	P <sub>av</sub>	100
Mission load power (W)	P <sub>pid</sub>	300
Propeller efficiency	η <sub>prop</sub>	0.82
Motor efficiency	η <sub>mot</sub>	0.90

GPM algorithms. Therefore, both the fixed constraint path and the point-to-point maximum solar radiation path schemes are compared to the respective benchmark schemes to demonstrate their potential. Specifically, the fixed-constrained 3D path scheme of [17] is cited as a benchmark.

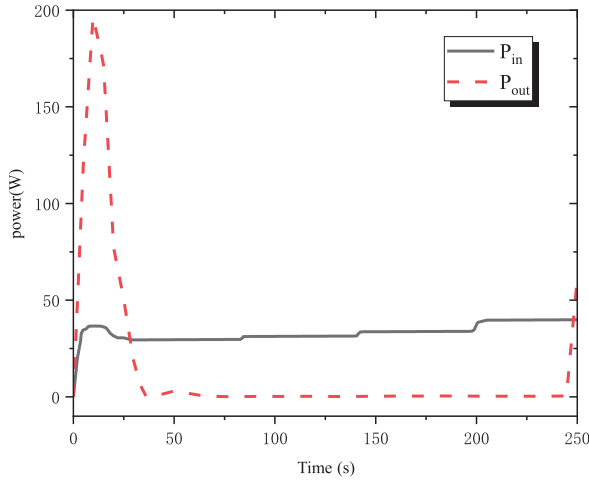


FIGURE 9.  $P_{in}$  and  $P_{out}$  in the optimization result.

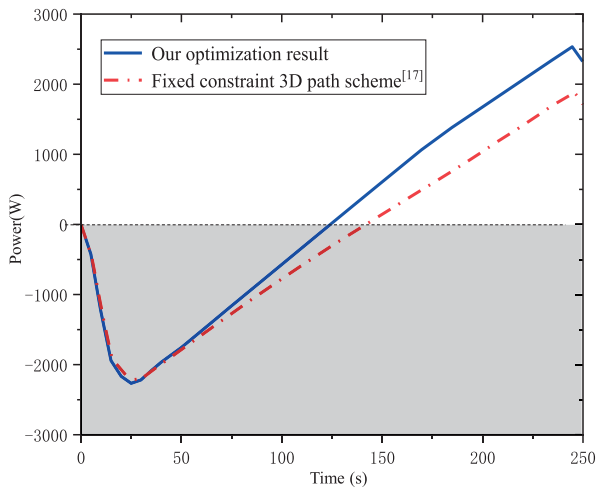


FIGURE 10. Net energy.

**A. COMPARISON WITH THE FIXED CONSTRAINT 3D PATH SCHEME**

1) VALIDATION

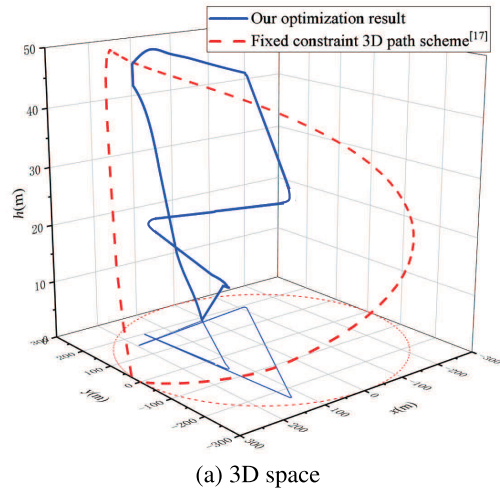
The papers [9], [17] have discussed flight path optimization for fixed target missions, where both of the methods fix the flight path on a cylindrical surface constrained by the scanning radius. Specifically, reference [17] uses a 3D path model, which is comparable to our research. To verify the point-to-point calculation method in Section III 2, this method is used to optimize and compare the same parameters as those in reference [17]. Therefore, the objective function of the multiobjective path optimization is changed to the objective function proposed in [17]:

$$\max : J = \int_{t_0}^{t_f} (P_{in} - P_{out})dt, \quad (21)$$

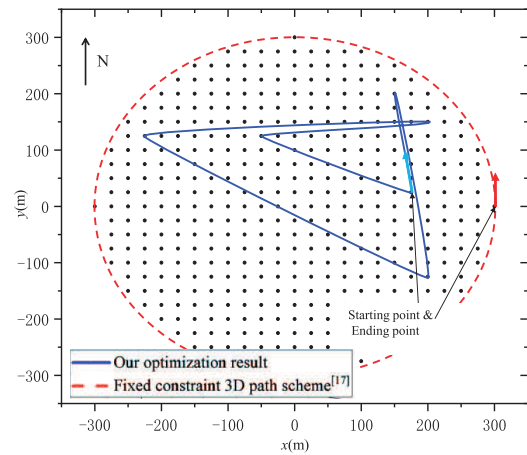
where  $P_{in} - P_{out}$  is the net energy. The virtual cylinder surface 3D model mentioned in [17] is adopted as a benchmark. For the sake of uniformity, the parameters of the aircraft model (Tab. 4) and simulation settings (Tab. 5) are exactly the same

TABLE 8. Constraints of the variables.

Parameter	Minimum value	Maximum value
h (km)	15	25
v (m/s)	25	80
SoC	0	1
$\gamma$	-3	2
t (h)	0	24
$\alpha$	-3	7



(a) 3D space



(b) Plane space

FIGURE 11. The path in 3D space and plane space.

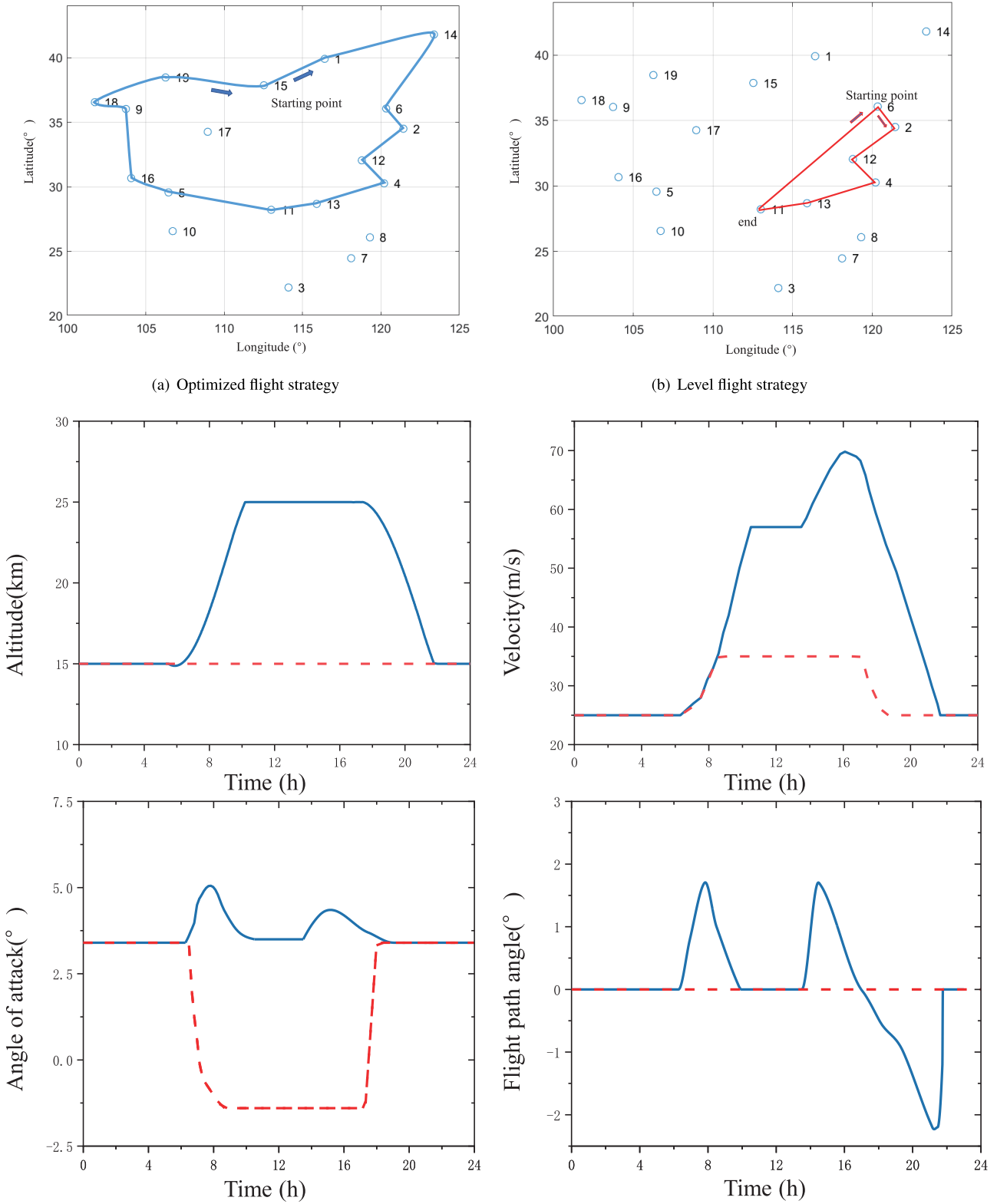
in reference [17]. One hundred points are uniformly set on a circle with a diameter of 300 meters, as shown in Fig. 6, and the point-to-point algorithm is used to fly around the circle as a validation case comparison.

As seen from Tab. 6 and Fig. 7, the comparison between the validation case and the result of Huang *et al.* in [17] shows that the relative error is less than five percent, with the maximum error occurring at 250 seconds. The results confirm the correctness of our method, but the error may be caused by a discontinuity at this point.

2) PRELIMINARY RESULT

To further verify the algorithm’s adaptability to scenes with higher degrees of freedom, evenly distributed points are gen-





(a) Optimized flight strategy

(b) Level flight strategy

(c) Altitude, velocity, flight path angle and attack angle comparison

**FIGURE 12.** Comparison of the optimized flight strategy and level flight strategy. The blue line represents the optimized flight strategy, and the red line represents the level flight strategy.

erated within a circle with a radius of 300 meters, as shown in Fig. 8. The point-to-point path optimization method is used to solve the maximum net energy path inside the cylinder but not on the surface of the cylinder.

The optimization results of  $P_{in}$  and  $P_{out}$  with point-to-point path optimization are shown in Fig. 9. Fig. 10 compares the net energy changes between the validation case and the optimization results. The results showed that the net energy increases after the optimization scheme is adopted. Fig. 11(a) shows a 3D path comparison between the optimization result and the case result, and Fig. 11(b) projects the 3D path into a plane. According to the results shown above, using the point-to-point path optimization algorithm can achieve automatic optimization in a certain area and find a path for obtaining more net energy.

### B. COMPARISON OF OPTIMIZED FLIGHT STRATEGY AND LEVEL FLIGHT STRATEGY

The algorithm proposed in this paper is used for performance analysis. The parameters of the aircraft model and the constraints of the variables are presented in Tabs. 7 and 8, respectively. In particular, the initial conditions are usually determined by the energy balance at the beginning of the cruise day. Based on the above simulation settings, the simulation analysis and comparison of the flight paths under different conditions are carried out.

Various studies [13]–[21] have discussed the necessity of using excess solar energy for climbing. First, the SP-UAV can use the potential energy of gravity to glide and reduce the weight of the carried battery. Second, the higher the flying height is, the more solar energy can be obtained. To verify the effectiveness of the climbing strategy using gravitational potential energy storage, the optimization algorithm proposed in this paper is compared with the horizontal flight strategy. Explicitly, the flight date is fixed on June 21.

Due to the altitude limitations, the level flight strategy can only accelerate to the maximum flight speed at the current altitude when the solar radiation is sufficient. As shown in Fig. 12(a) and Fig. 12(b), the lower flight speed results in a smaller scan path. Fig. 12(c) compares the changes in the altitude, speed, angle of attack, and flight angle of the two strategies. The results show that SP-UAV climbing flight can not only use gravitational potential energy storage to reduce the weight of the battery in the aircraft design stage but also improve the flight speed to achieve a longer scanning path. This is critical to the SP-UAV's mission. As seen from the total length of the path, the path length of the optimization result is almost twice as long as the horizontal flight strategy, which results in four times the scanning area. Then, the effectiveness of the proposed strategy is verified.

### C. COMPARISON OF OPTIMIZED FLIGHT STRATEGY AND FIXED LOCATION STRATEGY

To verify the influence of the flight location and the flight range on the flight strategy, a cross-region flight and three fixed-location flights are selected for comparison. According

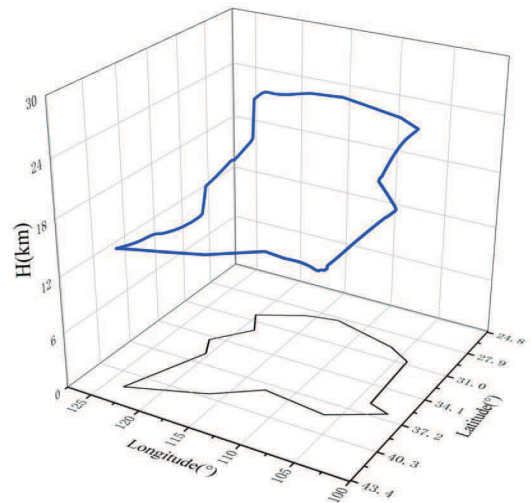


FIGURE 13. 3D path in optimized flight strategy.

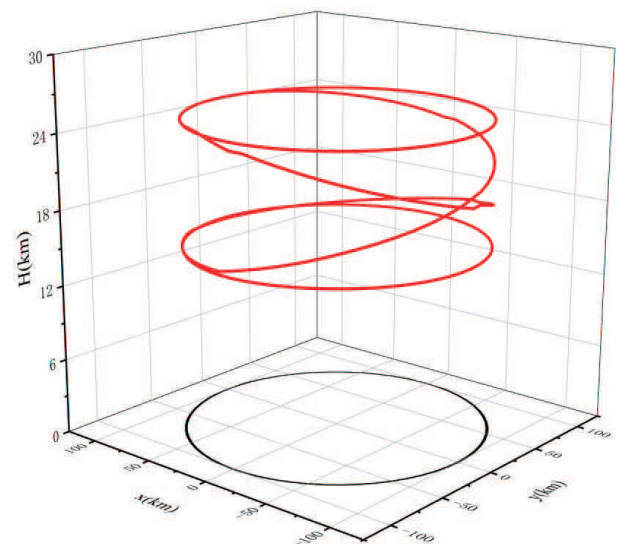


FIGURE 14. 3D path in fixed location strategy.

to the application scenario in this paper, the SP-UAV appears in different cities at different times of the day, and the optimization result is compared with a circle over a fixed city. Explicitly, the optimization is implemented in three flight regions: City 1 (116.40° N), City 2 (114.122.2° N), and City 3 (101.75 36.56° N), with the flight date set for June 21.

Suppose that the fixed-location flight strategy is to fly over a fixed city with a detection radius of 100 km over each city. Each flight strategy is divided into four phases (as described in section III.A), each of which satisfies the process constraints. Note that the results have been converted to local time. The results of the 3D flight trajectory using the optimized flight strategy are shown in Fig. 13, while Fig. 14 shows the 3D flight trajectory at a fixed location.

Figs. 15(a) and 15(b) compare the solar power and the total solar power at each moment. The maximum solar radiation intensity of 22° N is higher than those of 36° N and 40° N. However, the sunshine durations of 36° N and 40° N are longer, resulting in their total daily solar radiation being

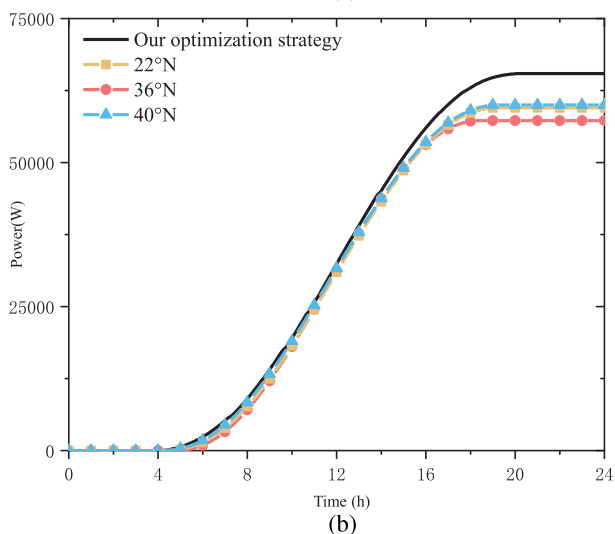
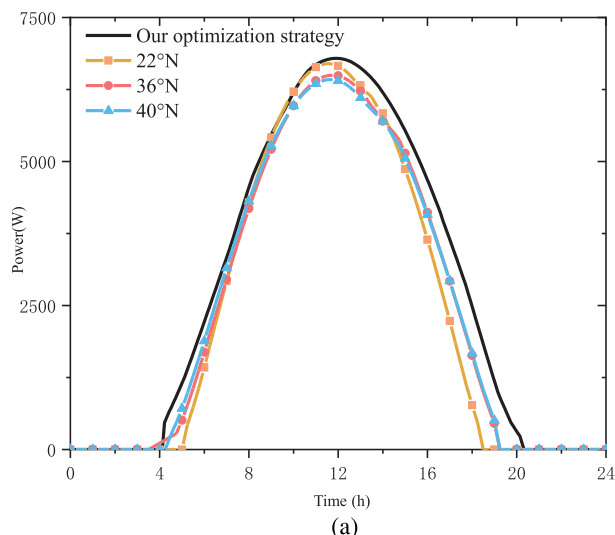


FIGURE 15. (a) Solar power. (b) Total solar power.

higher than that of 22° N. Compared with the optimization strategy, both the maximum solar radiation intensity and the daily total solar radiation are higher than the fixed-position flight results.

The results show that compared with the fixed-location flight strategy, cross-regional flight can obtain more solar energy and prolong the solar irradiation time. The optimization results indicate that the SP-UAV begins to climb from the east in the morning due to the early eastern sunrise. At noon, SP-UAV flies to low latitudes where the sun’s radiation is strong. In the afternoon, the SP-UAV flies to the west in pursuit of the longest hours of sunshine. Taking advantage of this feature to conduct information reconnaissance and other mission cruises not only expands the mission scope but also helps to increase the range.

**D. INFLUENCE OF THE FLIGHT SEASON ON THE OPTIMIZATION RESULTS**

To verify the impacts of different flight seasons on the flight strategy, a flight date in another flying season was selected:

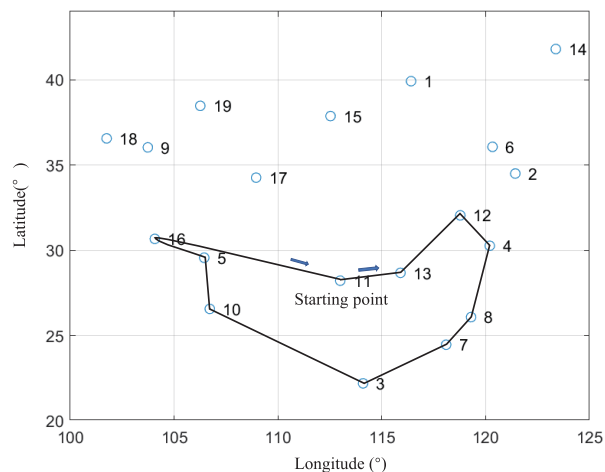


FIGURE 16. Flight date on March 20.

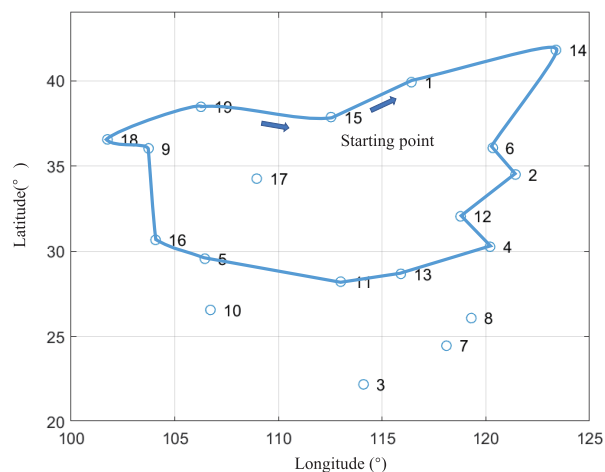


FIGURE 17. Flight date on June 21.

March 20. The results are shown in Figs. 16 and 17, where the optimization strategy has different characteristics under different flight dates. Compared with the optimization results on June 21, the solar irradiance on March 20 is lower. The results show that the starting point selected by the optimization algorithm is more southward and that the city latitude of the whole path is lower due to the southward movement of the direct sunlight. In addition, the number of cities on a flight cycle is reduced from 14 to 10 due to the reduced daylight during the day. Even if the intensity of the solar radiation decreases with changes in the seasons, the selection of the right flight strategy and flight position can still realize the full potential of the SP-UAV.

**V. CONCLUSION**

In this paper, a mission-oriented 3D path planning problem for maximizing the energy utilization of HALE solar-powered aircraft is studied. The comprehensive

optimization of GPM algorithms and the ant colony algorithm is applied to solve the mission path optimization problem for HALE solar-powered aircraft due to their advantages in solving coupling problems. By comprehensive utilization of the attitude angle and flight altitude and the definition of the objective functions for different phases of flight, the optimized flight strategy is able to increase the power of photovoltaic cells and improve mission cruise completion. Compared with the level flight strategy and the fixed-location flight strategy, the optimized flight strategy can obtain more solar energy.

This research focuses on how to maximize the use of solar energy for 3D path planning in higher freedom scenarios. The combination of the optimization algorithm with the overall design of the SP-UAV and the establishment of an SP-UAV design framework based on path energy optimization are potential future research directions. The following aspects are worth considering: (1) the improvement of the algorithm performance under more complicated scenarios and (2) the impact of environmental factors and further in-depth research.

## REFERENCES

- R. J. Boucher, "Sunrise, the worlds first solar-powered airplane," *J. Aircr.*, vol. 22, pp. 840–846, Oct. 1985.
- S. A. Montgomery and N. J. Mourtos, "Design of a 5 kilogram solar-powered unmanned airplane for perpetual solar endurance flight," in *Proc. 49th AIAA/ASME/SAE/ASEE Joint Propuls. Conf.*, San Jose, CA, USA, 2013, p. 3875.
- Y. Hu, Y. Yang, S. Li, and X. Ma, "Computational optimal launching control for balloon-borne solar-powered UAVs in near-space," *Sci. Prog.*, vol. 103, no. 1, pp. 1–19, Sep. 2019.
- Z. Xiongfeng, G. Zheng, and H. Zhongxi, "Solar-powered airplanes: A historical perspective and future challenges," *Prog. Aerosp. Sci.*, vol. 71, pp. 36–53, Nov. 2014.
- P. Panagiotou, I. Tsavlidis, and K. Yakinthos, "Conceptual design of a hybrid solar MALE UAV," *Aerosp. Sci. Technol.*, vol. 53, pp. 207–219, Jun. 2016, doi: 10.1016/j.ast.2016.03.023.
- J. Li, J. Liao, Y. Liao, H. Du, S. Luo, W. Zhu, and M. Lv, "An approach for estimating perpetual endurance of the stratospheric solar-powered platform," *Aerosp. Sci. Technol.*, vol. 79, pp. 118–130, Aug. 2018, doi: 10.1016/j.ast.2018.05.035.
- A. Klesh and P. Kabamba, "Energy-optimal path planning for solar-powered aircraft in level flight," in *Proc. AIAA Guid., Navigat. Control Conf. Exhib.*, Hilton Head Island, SC, USA, Aug. 2007, pp. 1–17.
- A. T. Klesh and P. T. Kabamba, "Solar-powered aircraft: Energy-optimal path planning and perpetual endurance," *J. Guid., Control, Dyn.*, vol. 32, no. 4, pp. 1320–1329, Jul. 2009.
- S. C. Spangelo and E. G. Gilbert, "Power optimization of solar-powered aircraft with specified closed ground tracks," *J. Aircr.*, vol. 50, no. 1, pp. 232–238, Jan. 2013.
- Y. Huang, H. Wang, and P. Yao, "Energy-optimal path planning for solar-powered UAV with tracking moving ground target," *Aerosp. Sci. Technol.*, vol. 53, pp. 241–251, Jun. 2016.
- J. Wu, H. Wang, N. Li, P. Yao, Y. Huang, Z. Su, and Y. Yu, "Distributed trajectory optimization for multiple solar-powered UAVs target tracking in urban environment by adaptive grasshopper optimization algorithm," *Aerosp. Sci. Technol.*, vol. 70, pp. 497–510, Nov. 2017.
- J. Wu, H. Wang, N. Li, P. Yao, Y. Huang, and H. Yang, "Path planning for solar-powered UAV in urban environment," *Neurocomputing*, vol. 275, pp. 2055–2065, Jan. 2018.
- X.-Z. Gao, Z.-X. Hou, Z. Guo, P. Wang, and J.-T. Zhang, "Research on characteristics of gravitational gliding for high-altitude solar-powered unmanned aerial vehicles," *Proc. Inst. Mech. Eng., G, J. Aerosp. Eng.*, vol. 227, no. 12, pp. 1911–1923, Dec. 2013.
- X.-Z. Gao, Z.-X. Hou, Z. Guo, R.-F. Fan, and X.-Q. Chen, "The equivalence of gravitational potential and rechargeable battery for high-altitude long-endurance solar-powered aircraft on energy storage," *Energy Convers. Manage.*, vol. 76, pp. 986–995, Dec. 2013.
- X.-Z. Gao, Z.-X. Hou, Z. Guo, X.-Q. Chen, and X.-Q. Chen, "Joint optimization of battery mass and flight trajectory for high-altitude solar-powered aircraft," *Proc. Inst. Mech. Eng., G, J. Aerosp. Eng.*, vol. 228, no. 13, pp. 2439–2451, 2014.
- X.-Z. Gao, Z.-X. Hou, Z. Guo, J.-X. Liu, and X.-Q. Chen, "Energy management strategy for solar-powered high-altitude long-endurance aircraft," *Energy Convers. Manage.*, vol. 70, pp. 20–30, Jun. 2013.
- Y. Huang, C. Jianguo, W. Honglun, and S. Guofeng, "A method of 3D path planning for solar-powered UAV with fixed target and solar tracking," *Aerosp. Sci. Technol.*, vol. 92, pp. 831–838, Sep. 2019.
- S. Wang, M. Dongli, and M. Yang, "Flight strategy optimization for high-altitude long-endurance solar-powered aircraft based on Gauss pseudo-spectral method," *Chin. J. Aeronaut.*, vol. 32, no. 10, pp. 2286–2298, 2019.
- J.-S. Lee and K.-H. Yu, "Optimal path planning of solar-powered UAV using gravitational potential energy," *IEEE Trans. Aerosp. Electron. Syst.*, vol. 53, no. 3, pp. 1442–1451, Jun. 2017.
- M. Sun, X. Ji, K. Sun, and M. Zhu, "Flight strategy optimization for high-altitude solar-powered aircraft based on gravity energy reserving and mission altitude," *Appl. Sci.*, vol. 10, no. 7, p. 2243, 2020, doi: 10.3390/app10072243.
- W. Zhu, J. Li, and Y. Xu, "Optimum attitude planning of near-space solar powered airship," *Aerosp. Sci. Technol.*, vol. 84, pp. 291–305, Jan. 2019, doi: 10.1016/j.ast.2018.10.007.
- L. Zhang, J. Li, Y. Jiang, H. Du, W. Zhu, and M. Lv, "Stratospheric airship endurance strategy analysis based on energy optimization," *Aerosp. Sci. Technol.*, vol. 100, May 2020, Art. no. 105794, doi: 10.1016/j.ast.2020.105794.
- M. Wu, Z. Shi, T. Xiao, and H. Ang, "Energy optimization and investigation for Z-shaped sun-tracking morphing-wing solar-powered UAV," *Aerosp. Sci. Technol.*, vol. 91, pp. 1–11, Aug. 2019, doi: 10.1016/j.ast.2019.05.013.
- M. Wu, Z. Shi, H. Ang, and T. Xiao, "Theoretical study on energy performance of a stratospheric solar aircraft with optimum  $\wedge$ -shaped rotatable wing," *Aerosp. Sci. Technol.*, vol. 98, Mar. 2020, Art. no. 105670, doi: 10.1016/j.ast.2019.105670.
- J. A. Duffie and W. A. Bechman, *Solar Engineering of Thermal Processes*. Hoboken, NJ, USA: Wiley, 2006.
- B. Keidel, "Auslegung und Simulation von Hochfliegenden Dauerhaft Stationierbaren Solardrohnen," Ph.D. dissertation, Technischen Universität München Fakultät für Maschinenwesen, München, Germany, 2000.
- K. Katiyar and K. Pandey, "A review of solar radiation models—Part I," *J. Renew. Energy*, vol. 2013, pp. 1–11, Dec. 2013.
- D. Garg, M. Patterson, and W. W. Hager, "A unified framework for the numerical solution of optimal control problems using pseudospectral methods," *Automatica*, vol. 46, pp. 1843–1851, Nov. 2010.
- M. M. Hosseini, "A modified pseudospectral method for numerical solution of ordinary differential equations systems," *Appl. Math. Comput.*, vol. 176, pp. 470–475, May 2006.
- W. K. Foong, A. R. Simpson, H. R. Maier, and S. Stolp, "Ant colony optimization for power plant maintenance scheduling optimization—A five-station hydropower system," *Ann. Oper. Res.* vol. 159, no. 1, pp. 433–450, 2008.
- P. S. Shelokar, V. K. Jayaraman, and B. D. Kulkarni, "An ant colony classifier system: Application to some process engineering problems," *Comput. Chem. Eng.*, vol. 28, no. 9, pp. 1577–1584, 2004.
- M. Dorigo, V. Maniezzo, and A. Colnori, "Positive feedback as a search strategy," Dept. Electron., Politecnico di Milano, Milan, Italy, Tech. Rep. 91-016, 1991.
- Z. Zhen, Y. Chen, L. Wen, and B. Han, "An intelligent cooperative mission planning scheme of UAV swarm in uncertain dynamic environment," *Aerosp. Sci. Technol.*, vol. 100, May 2020, Art. no. 105826, doi: 10.1016/j.ast.2020.105826.
- K. L. Hoffman, M. Padberg, and G. Rinaldi, *Traveling Salesman Problem*. Boston, MA, USA: Springer, 2013, pp. 1573–1578.
- M. Dorigo and L. M. Gambardella, "Ant colonies for the traveling salesman," *Biosystems*, vol. 43, no. 2, pp. 73–81, 1997.
- M. Dorigo and L. M. Gambardella, "Ant colony system: A cooperative learning approach to the traveling salesman problem," *IEEE Trans. Evol. Comput.*, vol. 1, no. 1, pp. 53–66, Apr. 1997.



**XIANGYU WANG** received the B.S. degree from the Department of Energy and Power Engineering, Tsinghua University, in 2016. He is currently pursuing the Ph.D. degree in flight vehicle design with the Institute of Engineering Thermophysics, Chinese Academy of Science, Beijing, China.

His research interests include UAV systems, flight control law design, and path planning. He is also investigating the project “Overall design and path planning of solar-powered UAVs.”



**DI WU** received the bachelor’s and master’s degrees in aircraft design from Northwestern Polytechnical University, in 2011 and 2014, respectively, and the Ph.D. degree from The Hong Kong University of Science and Technology, in 2018.

From 2018 to 2020, he has served as an Assistant Researcher for the Institute of Engineering Thermophysics, Chinese Academy of Sciences, Beijing, China. His research interests include low Reynolds number aerodynamics, aircraft dynamics and control, and aerodynamic noise.



**ZIJIAN ZHANG** received the bachelor’s, master’s, and Ph.D. degrees in aircraft design from Northwestern Polytechnical University, in 2003, 2006, and 2009, respectively.

From 2009 to 2017, he has served as an Assistant Researcher and an Associate Researcher for the UAV Institute, Northwestern Polytechnical University. From 2018 to 2019, he has also served as a Project Researcher for the Institute of Engineering Thermophysics, Chinese Academy of Sciences, Beijing, China. He successively published more than ten scientific articles as the first author, seven of which were indexed by EI/SCI/ISTP/SSCI, and applied for five invention patents. His research interests include overall aircraft design, aircraft dynamics and control, flight simulation, and aircraft aeroelasticity/aero-servoelasticity.



**YANPING YANG** (Member, IEEE) received the B.S. degree in automation and the M.S. degree in electronics engineering from Xidian University, Xi’an, China, in 2008 and 2013, respectively. Thereafter, he studied at the Department of Electronic Engineering, Tsinghua University, and also received the Ph.D. degree from the National Digital Switching System Engineering and Technological Research and Development Center, Zhengzhou, China.

He is currently a Postdoctoral Researcher with the Institute of Engineering Thermophysics, Chinese Academy of Science, Beijing, China. His research interests include UAV formation flight, UAV systems, flight control law design, wireless communications, cognitive radio networks, and network coding. He has published more than 20 articles regarding his research interests, including IEEE TRANSACTIONS ON COMMUNICATIONS (TCOM), IEEE TRANSACTIONS ON VEHICULAR TECHNOLOGY (TVT), and IEEE ACCESS. He has served on the TPC of IEEE WCSP 2019 and as a reviewer for IEEE JOURNAL ON SELECTED AREAS IN COMMUNICATIONS (JSAC), IEEE TRANSACTIONS ON COMMUNICATIONS (TCOM), IEEE TRANSACTIONS ON VEHICULAR TECHNOLOGY (TVT), ICC, and GlobeCom.



**XIAOPING MA** received the bachelor’s, master’s, and Ph.D. degrees in aircraft design from Northwestern Polytechnical University, in 1983, 1988, and 2008, respectively.

He has been involved in the research and development of UAV systems for a long time and has served as the deputy chief engineer and a chief engineer for various types of UAVs. He has published more than 20 articles related to UAV designs, among which five were retrieved by EI/SCI/ISTP/SSCI. His research interests include UAV systems, aircraft and structure design, launching and recovering techniques, and system flight tests. He also serves as a Senior Member for the Aviation Society of China. He has won the first prize and the second prize of National Science and Technology Progress; the second prize of the National Commission of Science, Technology and Industry for National Defense; and the first prize and the second prize of the Ministerial awards.

...